ELSEVIER

Journal of Chromatography A, 691 (1995) 37–53

JOURNAL OF CHROMATOGRAPHY A

Optical properties of axial-illumination flow cells for simultaneous absorbance–fluorescence detection in micro liquid chromatography

Ahmad A. Abbas, Dennis C. Shelly*

Department of Chemistry and Biochemistry, Texas Tech University, Lubbock, TX 79409-1061, USA

Abstract

Simultaneous measurements of absorbance and fluorescence are possible with axial-illuminated flow cells, fashioned with a unique bend geometry. The optical properties of these flow cells have been studied. Effects of variations in lumen refractive index, capillary wall thickness and physical pathlength have been examined. A theoretical understanding of the various light propagation modes and of light intensity distributions in these modes, based upon lumen refractive index, has been attained. Of more practical significance, optical pathlengths from < 1 cm to 6 cm are simply attained by positioning the inlet optical fiber along the capillary axis with respect to the bend. The flow cell volumes obtained with different combinations of capillary I.D. and optical pathlength make the flow cell and resulting detector compatible with conventional HPLC and microscale separations. Also, studies have been performed to determine the effects of increased optical pathlength on overall analytical separation efficiency and detectability in the analysis of polynuclear aromatic hydrocarbons using laser-induced fluorescence micro-LC.

1. Introduction

Microcolumn separation techniques, such as micro-LC and capillary electrophoresis, have gained considerable interest during the past decade [1–3]. These techniques have provided extremely high separation efficiencies and rapid analyses, compared to conventional methods. In order to exploit these advantages, it is necessary to minimize extracolumn dispersion, particularly in connecting tubes and at the detector. "On-column" detection techniques [4–6], utilizing cross-capillary illumination of the actual micro-column, provide the lowest extracolumn dispersion. Also, post-column, cross-capillary illumination has provided acceptable performance for UV absorbance [7,8] and fluorescence [9,10] detection in micro-LC. Various flow cell and illumination options for laser-induced fluorescence detection have been reviewed [11,12]. Though quite reasonable detection limits have been reported with these detection schemes, the small optical pathlengths (50–250 μm) result in very small illuminated volumes. This limits absorbance and fluorescence signal intensities and prevents detection of solutions with low concentrations, e.g. high concentration limits of detection.

Illuminating a capillary flow cell along its axis (axial illumination) is one way to increase the pathlength for optical detection [13–27]. It is achieved by focussing light with a lens (convex lens, ball lens, etc) [13,16–22,25,26] or inserting

* Corresponding author.

0021-9673/95/$09.50
SSDI 0021-9673(94)01036-6

a light-guiding optical fiber directly into the capillary flow cell [14,24]. Once light enters the capillary, it propagates by total internal reflection, external reflection and refraction at the wall–air and/or wall–lumen interface, thus confining its energy within the outer wall boundaries of the capillary [28]. A lensless, externally mirrored capillary flow cell has been reported [27].

Various axial-illumination flow cell designs have recently been developed in order to improve the concentration sensitivity of detectors for micro-LC and capillary electrophoresis. The importance of eliminating mechanical vibrations and the necessity for smooth coupling of source light into the capillary flow cells (50–250 μm I.D) are some of the most important design considerations. Abbas and Shelly [25] coupled laser light inside a 150 μm I.D capillary flow cell (pathlength 1 cm) using a convex lens with a unique nebulizer orifice. This device eliminated solvent droplet formation at the exit end of the flow cell, enabling efficient coupling of incident laser light into the capillary and approximately $1 \cdot 10^{-10}$ M concentration detectability for aflatoxins. Also, Chervet and co-workers [16,22] constructed a capillary "Z shaped" flow cell (pathlength 3 mm) for micro-LC with UV absorbance detection. The "Z" cell was merely interposed between the source and the transducer. There was no "coupling" in actuality [16,22]. This produced very low light transmission in the flow cell capillary, mainly due to the large fraction of light refracting out of the capillary, before reaching the detector. This resulted in high background noise and low signal-to-noise ratio (S/N). Moring and Reel [26] reported improvements in the absorbance S/N (minimum detectable concentration, MDC, of 10^{-8} M), by coupling light with sapphire ball optics into the "Z" cell. Taylor and Yeung [24] inserted a 46-μm light-guiding optical fiber into a 75 μm I.D. capillary for laser-induced fluorescence detection in capillary electrophoresis. Concentration detection limits ($S/N = 3$) of between $1 \cdot 10^{-11}$ and $6 \cdot 10^{-12}$ M were reported for Rhodamine 6G. A 7-nl multireflection flow cell has been developed by Wang et al. [27]. In this device, a straight externally mirrored capillary is illuminated through the wall at an angle sufficient to cause multiple cross-capillary reflections, over a total linear distance of less than 1.5 mm. Substantial increases in sensitivity (40 ×) and pathlength (44 ×) were reported for absorbance detection in capillary electrophoresis. A concentration limit of detection of $3 \cdot 10^{-7}$ M for Brilliant Green was reported.

Most of this micro-LC detector development work has resulted in flow cells/detectors that enable single-parameter measurement. This does not fully utilize the available optical information. Also, many analytes may not be detected under optimum conditions in single-parameter sensing. Consequently, there is a need for simultaneous measurement of more than one signal (absorbance, fluorescence, refractive index, etc.). Consider the TriDet, trifunctional detector for conventional HPLC [29], which permits simultaneous absorbance, fluorescence and conductivity measurements. Multiparameter detection can provide much greater overall detectability and also generate more information about a particular analyte in a single chromatographic experiment. To the best of our knowledge, there has only been one report of multiparameter optical detection for miniaturized LC, namely simultaneous absorbance, fluorescence and refractive index microbore LC [30] using a "rather large" 1-μl flow cell.

In this paper we show how light-propagation characteristics of a unique bent capillary flow cell can be exploited for multiparameter optical detection. A description of the design and operation of the simultaneous absorbance–fluorescence capillary flow cell and detector are presented. The dependence of absorbance and fluorescence signal intensities on lumen refractive index ($n_1 = 1.3587$–1.4940), physical pathlength (1–5.8 cm) and capillary wall thickness (65–271 μm) are discussed in detail. Finally, we examine the combined influence of fluorescence optical window length on detectability and separation efficiencies for a model reversed-phase micro-LC separation of polynuclear aromatic hydrocarbons.

2. Theory

In order to obtain a large optical signal (absorbance, fluorescence, etc), the analyte must interact with most of the incident light energy. For capillaries, this is possible if most of the incident light is present in the lumen, as opposed to the wall of the capillary. Light distribution in the wall and the lumen depend on various factors such as the method used to introduce light into the capillary (as discussed in the Introduction), ratio of the lumen and wall refractive indices and lumen and wall thicknesses. Tsunoda and coworkers [14,15] used statistical methods such as Markov chain and Monte Carlo simulations to show that a propagating photon (ray) will spend half of its time in the lumen and half in the wall, for a particular capillary dimension (wall and lumen thickness) and lumen/wall refractive indices. In our previous work [25] we used a ray trace diagram approach to analyze the light propagating pathways inside a capillary flow cell. Results obtained therein, using Snell's law and simple trigonometric functions, showed the effects of lumen refractive index on effective pathlength, for any propagating ray. We also found that the calculated effective pathlength was smaller than the physical pathlength of the capillary flow cell, when ray propagation occurred via pathway C (light propagation in the capillary wall *and* lumen), under the conditions used. The effective pathlength would exceed the physical pathlength *only* when pathway B (light propagation only in the capillary lumen) was the major light propagating pathway. We also observed that effective numerical aperture of the capillary increased with lumen refractive index and we concluded that this was partly responsible for increased fluorescence signals for higher mobile phase refractive indices. Strictly speaking, this change in numerical aperture is justified only for point source illumination at the lumen face. Since the lens defined the entrance cone to be smaller than this aperture, there must have been a different reason for these observations. Also, a complete description of light propagation was not achieved, as neither the angular distribution of incident light rays nor the complicating influence of lumen refractive index were taken into account.

In the present paper we have used Fresnel's equations [28] to obtain the values of reflectance and transmittance of a light ray at the lumen–wall and wall–air interfaces. In this scenario externally reflected rays remain within the lumen and refracted rays are transmitted out of the lumen. These equations provide a means for determining the fraction of a light ray that is distributed in the wall and the lumen of the capillary after striking such an interface. Eqs. 1 and 2 are Fresnel's equations for a lumen-propagating light ray, incident at the lumen–wall interface;

$$r_{sl} = -\sin(\phi_L - \phi_w)/\sin(\phi_L + \phi_w) \quad (1)$$

$$r_{pl} = \tan(\phi_L - \phi_w)/\tan(\phi_L + \phi_w) \quad (2)$$

where r_{sl} and r_{pl} are the reflection coefficients for the perpendicular and parallel components of light approaching the lumen/wall interface from the lumen and ϕ_L and ϕ_w are the angles as shown in Fig. 1. When a light ray approaches the lumen–wall interface, after propagating in the wall, the reflection coefficients for the perpendicular and parallel components are given as r_{sw} and r_{pw}, respectively, as shown below

$$r_{sw} = \{\cos(\phi_w) - [(n_l/n_w)^2 - \sin(\phi_w)^2]^{1/2}\}/\{\cos(\phi_w) + [(n_l/n_w)^2 + \sin(\phi_w)^2]^{1/2}\} \quad (3)$$

$$r_{pw} = \{(n_l/n_w)^2 \cos(\phi_w) - [(n_l/n_w)^2 - \sin^2(\phi_w)]^{1/2}\}/\{(n_l/n_w)^2 \cos(\phi_w) + [(n_l/n_w)^2 - \sin^2(\phi_w)]^{1/2}\} \quad (4)$$

where n_l and n_w are the lumen and the wall refractive indices, respectively. Since we used an unpolarized light source, the reflectance, R, of a particular light ray is the average reflectance of

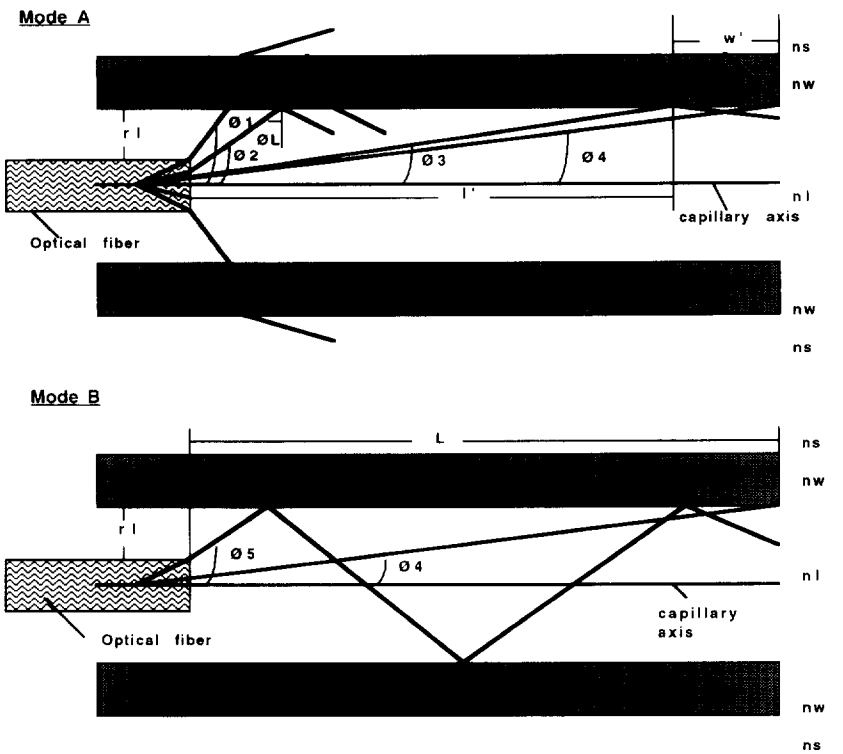

Fig. 1. Light propagation modes inside a capillary. n_s, n_w and n_l are the refractive indices of the medium surrounding the capillary, capillary wall and the lumen, respectively. r_l and r_w are half the lumen and wall thickness, respectively. The dark lines represent the different angled rays of light incident inside the capillary. l', w' and L are the distances as shown.

the parallel and the perpendicular components [28] and is given as

$$R_l = 0.5\left(r_{sl}^2 + r_{pl}^2\right) \quad (5)$$

$$R_w = 0.5\left(r_{sw}^2 + r_{pw}^2\right) \quad (6)$$

Fig. 1 shows ray trace diagrams for the different types of light propagation modes that are present in an axial-illumination capillary flow cell. These are correctly grouped into two categories, mode A and mode B, which exist according to inequalities 7 and 8 as

$$\text{Mode A: } n_l < n_w / \sin \phi_L \quad (7)$$

$$\text{Mode B: } n_l > n_w / \sin \phi_L \quad (8)$$

As shown in Fig. 1, at any instant in time, light energy is completely confined to the lumen if mode B is the light-propagating mode or light is distributed in both the wall and the lumen if mode A is observed. Let us consider each mode individually.

2.1. Mode A

This mode of light propagation can be divided into four submodes. Each submode is defined by finite angular light ray distributions according to the boundary conditions:

Mode A1: $\phi_1 \geq \phi > \phi_2$

Mode A2: $\phi_2 \geq \phi > \phi_3$

Mode A3: $\phi_3 \geq \phi > \phi_4$

Mode A4: $\phi_4 \geq \phi \geq 0$

Mode A1

For most chromatographic mobile phase (refractive indices, n_1, >1.2) and optical fiber (numerical aperture, NA, ≤ 0.8) combinations this mode does not exist. In this mode light rays refract out of the capillary at the wall–air interface since the angle that all light rays make at this interface (ϕ_w) will always be less than ϕ_{wc}, the critical angle for light to internally reflect at the wall–air interface. Obviously, this is a "lossy" mode. With proper selection of lumen refractive index and fiber numerical aperture, this mode can be completely eliminated. Using Snells law (see [28]) ϕ_{wc}, ϕ_1 and ϕ_2 can be calculated as shown below.

$$\phi_{wc} = \sin^{-1} (n_s/n_w) \quad (9)$$

$$\phi_1 = \sin^{-1} (\mathrm{NA}/n_1) \quad (10)$$

$$\phi_2 = \pi/2 - \sin^{-1} (n_s/n_1) \quad (11)$$

where n_s is the refractive index of the medium surrounding the capillary (air). Unlike mode A1, modes A2–A4 are the capillary-confined modes.

Mode A2

Mode A2 is the main light propagating mode (containing 97–98% of total light energy) when $n_1 < n_w$. When a ray of light that is within the confined angular boundaries supporting this mode (see above), is incident on the lumen–wall interface, two optical phenomena occur simultaneously. The light ray is refracted into the wall and externally reflected back into the lumen, as noted above using Fresnel's theory. Similarly, when a ray of light in the wall is incident on the lumen–wall interface, external reflection at the wall and refraction into the lumen occur simultaneously. Unlike mode A1 all the light rays incident at the wall–air interface are internally reflected back into the capillary. These processes repeat as the light ray propagates along the capillary. Variation of lumen refractive index will alter the fraction of light energy that is refracted and externally reflected at each interface. Fortunately, this can be calculated using Eqs. 1–6. The lower angular cutoff for mode A2 is an angle less than ϕ_3, where ϕ_3 is the angle for which $l' + w' = L$. Here, the propagating light ray, after penetrating the wall, will never reenter the lumen. l' and w' are given in Eqs. 12 and 13.

$$l' = r_1/\tan \phi_3 \quad (12)$$

$$w' = 2r_w \tan \left[\sin^{-1} (n_1/n_w \cos \phi_3)\right] \quad (13)$$

where r_1 and r_w are half the lumen and the wall thicknesses, respectively.

Modes A3 and A4

When n_1 is small compared to n_w only a very small fraction of light energy will propagate in mode A3. The angular distribution of light rays in mode A3 increases with lumen refractive index. Fresnel's equations can be used to find the fraction of light externally reflected in the lumen and refracted into the wall, for mode A3. Mode A4 is a single pass mode and is strictly dependent on r_1 and L (physical pathlength of the capillary flow cell). It is composed of a very small fraction of the total light rays. ϕ_4 defines the upper boundary and is given by Eq. 14

$$\phi_4 = \tan^{-1} (r_1/L) \quad (14)$$

2.2. Mode B

When light is incident at the lumen–wall interface, having been launched from an optical fiber with numerical aperture NA, and inequality 8 is satisfied, light will propagate as mode B (see Fig. 1). The angle at which *all* light is reflected back into the lumen (total internal reflection) is defined as ϕ_c. ϕ_c is given by inequality 15.

$$\phi_c \geq \sin^{-1} (n_w/n_1) \quad (15)$$

We can define an angle $\phi_{1'}$ such that $\phi_{1'} = \pi/2 - \phi_1$. ϕ_1 is defined in Eq. 10 and represents the largest angle of the light ray emitted by the fiber. For mode B to occur $\phi_{1'}$ must be greater than or equal to ϕ_c. Using a graphical mathematical computing program, MathCAD (Mathsoft, Seattle, WA, USA), we found that the lumen refractive index at which mode B occurs lies between

1.471 and 1.472. The numerical aperture for these calculations was chosen to be 0.2. The number of reflections in the lumen is maximized when n_l is at least equal to $n_w/\sin \phi_L$ and decreases as the lumen refractive index increases further.

Fig. 2 is a graphic representation of the behavior of Fresnel's equations over a wide range of lumen refractive indices, satisfying mode A. The variation of reflectance (R_l) and transmittance ($T_l = 1 - R_l$) of a light ray at the lumen–wall interface for n_l from 1.359 to 1.494 is shown in Fig. 2. Reflectance decreases with n_l up to 1.458, where it equals zero. Here, $n_l = n_w$. Thus a hollow cylindrical lightguide (capillary flow cell) behaves as a solid cylindrical lightguide (step index optical fiber). Further increases in n_l lead to a much higher reflectivity, hence a larger distribution of light in the lumen. This continues until $n_l \geq n_w/\sin \phi_L$ where light is totally reflected back into the lumen. At this point a transformation of the externally reflected mode (of mode A2) to the totally internally reflected mode (mode B) occurs (not shown in figure).

Consider that a beam of light is actually composed of a large number of rays incident at the interface and that each ray will have some fraction of its light distributed in the wall and the lumen of the capillary, determined by Fresnel's equations. Rays with small inclination, with respect to the capillary axis, will distribute more of their incident light into the externally reflected mode, compared to the refracted mode. As the angle increases, the fraction of light in the externally reflected mode decreases (decreasing reflectance). This confirms that axial-illumination flow cells are highly directional under optimal conditions suitable for reversed-phase micro-LC.

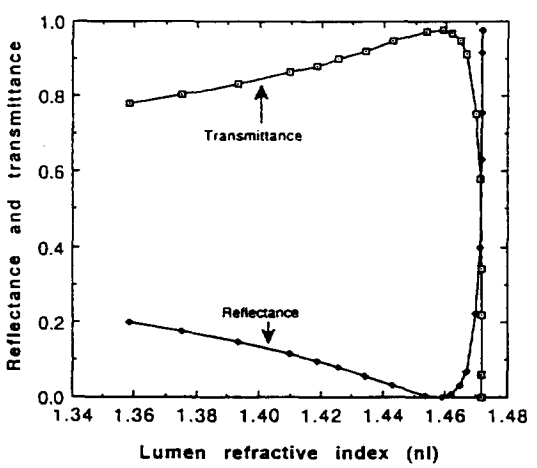

Fig. 2. Theoretically generated curve for reflectance and transmittance at the lumen–wall interface. For computation NA = 0.2 and $n_w = 1.458$.

3. Experimental

3.1. Capillary flow cell

Two types of bent flow cells were fabricated using fused-silica capillaries (Polymicro Technologies, Phoenix, AZ, USA). Fig. 3 shows photographs of the bend geometries, eccentric (a) and 90° (b) immediately after bend formation. A jig, containing a razer blade that was attached to metal clamps, and a butane microtorch were used to reproducibly bend the fused-silica capillaries. Fig. 3c and d shows light exiting at the bends of water-filled capillaries. These photographs were obtained with a 35 mm camera that was equipped with a $f/1.2$ lens. Water vapor from a dry ice–water bath was used to visualize the He–Ne laser (Melles Griot, Irvine, CA, USA) light Each of the two straight portions of the flow cells were about 7 cm long.

3.2. Simultaneous absorbance–fluorescence detector

Fig. 4 is a diagram that illustrates the operating principles of the simultaneous absorbance and fluorescence detector flow cell. Note the overall flow cell geometry, as described above. A block diagram of the entire instrument is shown in Fig. 5. A Model 487C Xenon cold fountain lamp (Karl Storz Endoscopy-America, Los Angeles, CA, USA) was used as the optical source. Wavelength selection was achieved with a $f/3.5$ grating monochromator (Optical Technology Devices, Elmsford, NY, USA). Light from the monochromator was focused into two 116-μm core diameter optical fibers (Polymicro

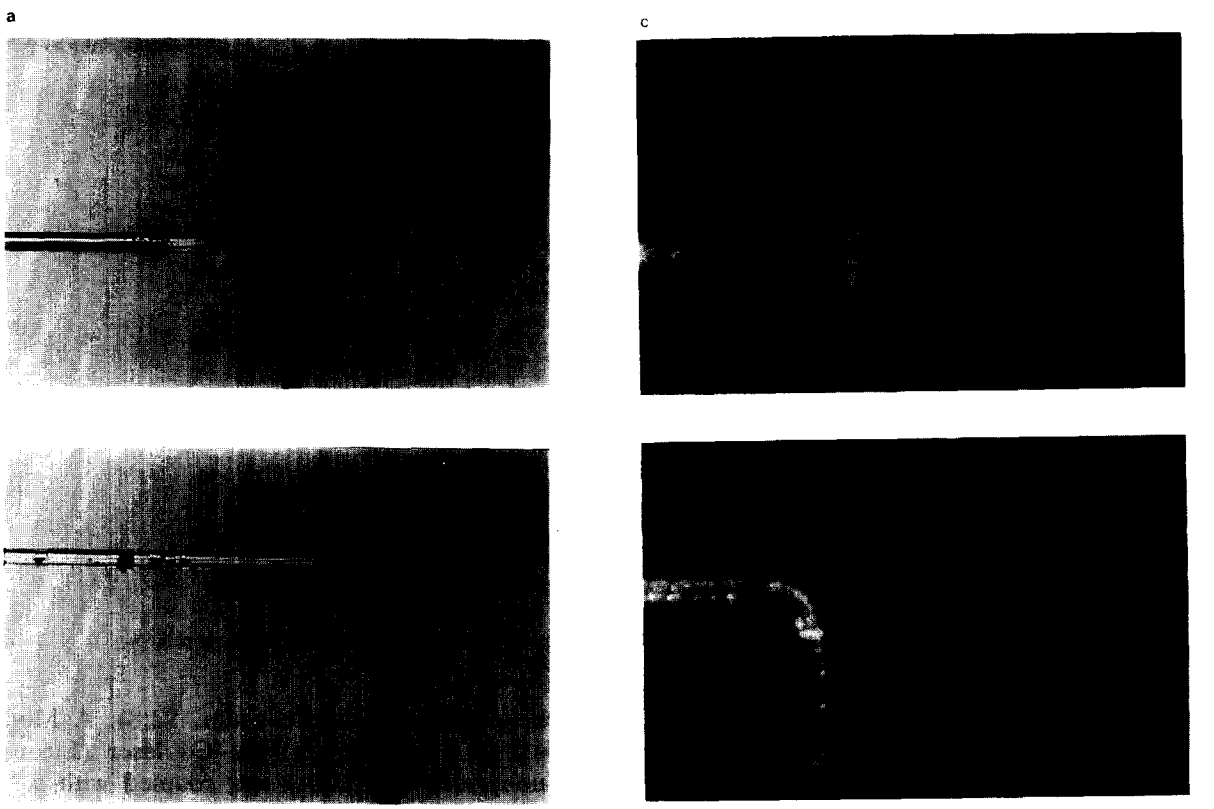

Fig. 3. Photographs of bent fused-silica capillaries (250 μm I.D. × 345 μm O.D.). (a) and (b) represent the eccentric and the 90° bend capillary flow cells, respectively. He–Ne laser light decoupled at the eccentric and 90° bend capillaries are shown in (c) and (d), respectively. In all cases the lumen contained water.

Technology) using a biconvex lens (Edmund Scientific, Barrington, NJ, USA). Two, nearly identical, 250 μm I.D, fused-silica eccentric bend capillaries were used as sample and reference cells. The optical fibers were inserted inside these capillaries, as shown in Fig. 4, and the pathlength of the detector window was adjusted by simply moving the optical fiber inside the capillary. Note that mobile phase enters at the arm opposite to that of the optical fiber; therefore, the optical fiber enters at the mobile phase exit of the capillary cell. Silicon photocells (Electronic Goldmine, Scottsdale, AZ, USA) were used as absorbance detector optical transducers. The capillary bends were positioned 1.5 mm from each detector, such that the exiting cone of light illuminated the entire face of the photocells. The fluorescence optical window was formed by removing the polyimide coating from a 2.4-cm length portion adjacent to the bend, using hot concentrated sulfuric acid. Fluorescence from this optical window was then imaged onto a Model R928 photomultiplier tube (PMT) (Hamamatsu, Bridgewater, NJ, USA), operated at 900 V. The emission optics consisted of a $f/1.5$ cylindrical lens (Melles Griot) and plastic sheet-type long-pass (>480 nm) cut-off filters (Roscolux, Port Chester, NY, USA). The mounting of optics and optoelectronics was accomplished by glueing Lego blocks of various shapes (Lego Systems, Enfield, CT, USA) into the appropriate geometries. Both photocells were electronically connected to a Model 757N log ratio amplifier (Analog Devices, Norwood, MA, USA) whose output was then digitized by a Model DT-2805 A/D board (Data Translation, Marlboro, MA,

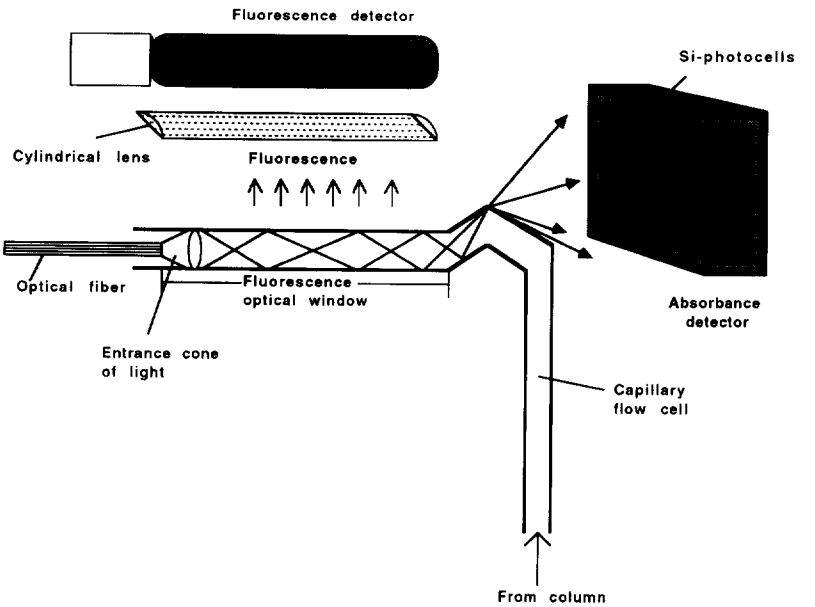

Fig. 4. Functional diagram of the simultaneous absorbance–fluorescence detector flow cell.

USA) and stored in a XT-class computer for further data analysis. Similarly for fluorescence, the analog output from the PMT was amplified with the electrometer from an Aminco Fluoromonitor HPLC detector (SLM-Aminco, Urbana, IL, USA) and digitized with a separate A/D–computer combination.

3.3. Micro-LC

Seven component polynuclear aromatic hydrocarbon mixtures were separated using reversed-phase micro-LC. A 250 μm I.D. fused-silica capillary (Polymicro Technologies), was packed with Spherisorb ODS2 (5 μm) particles (Alltech, Deerfield, IL, USA) using a computer controlled pump [31]. The length of the column used was 45 cm. A Model 8500 syringe pump (Varian Associates, Walnut Creek, CA, USA) was used for mobile phase delivery; 10-s sample injections were performed using a C14W microinjector (Valco, Houston, TX, USA) that was equipped with a 100-nl internal loop. All injections were of the moving loop type. The polynuclear aromatic hydrocarbon mixture was prepared by dissolving the sample in filtered (0.2-μm membrane) mobile phase (acetonitrile–water, 92:8). A Model 4412 B UV (325 nm) He–Cd laser (Liconix, Sunnyvale, CA, USA) was coupled with a 50-μm core diameter optical fiber using a $f/1.9$ planoconvex quartz lens (Oriel, Stanford, CT, USA) and an optical fiber positioner (Newport, Irvine, CA, USA). The other end of this fiber was then inserted into a low-volume capillary flow cell (99 μm I.D., 66 μm wall thickness), transferring approximately 40 μW (5.2 mW total laser power) into the flow cell. Fluorescence was measured with the R928 PMT, operated at 900 V. A 2-cm pathlength liquid filter, containing saturated aqueous cobalt sulfate, was used to minimize continuous emission from the laser. A 380-nm long-pass filter, a 385–488-nm band pass filter (both from Oriel) and a cylindrical lens ($f/1.5$, Melles Griot) were used as emission optics.

3.4. Data analysis

All chromatographic signals were analyzed using DADiSP 32 (DSP Development, Cambridge, MA, USA) digital signal processing software. Various operations, such as determination

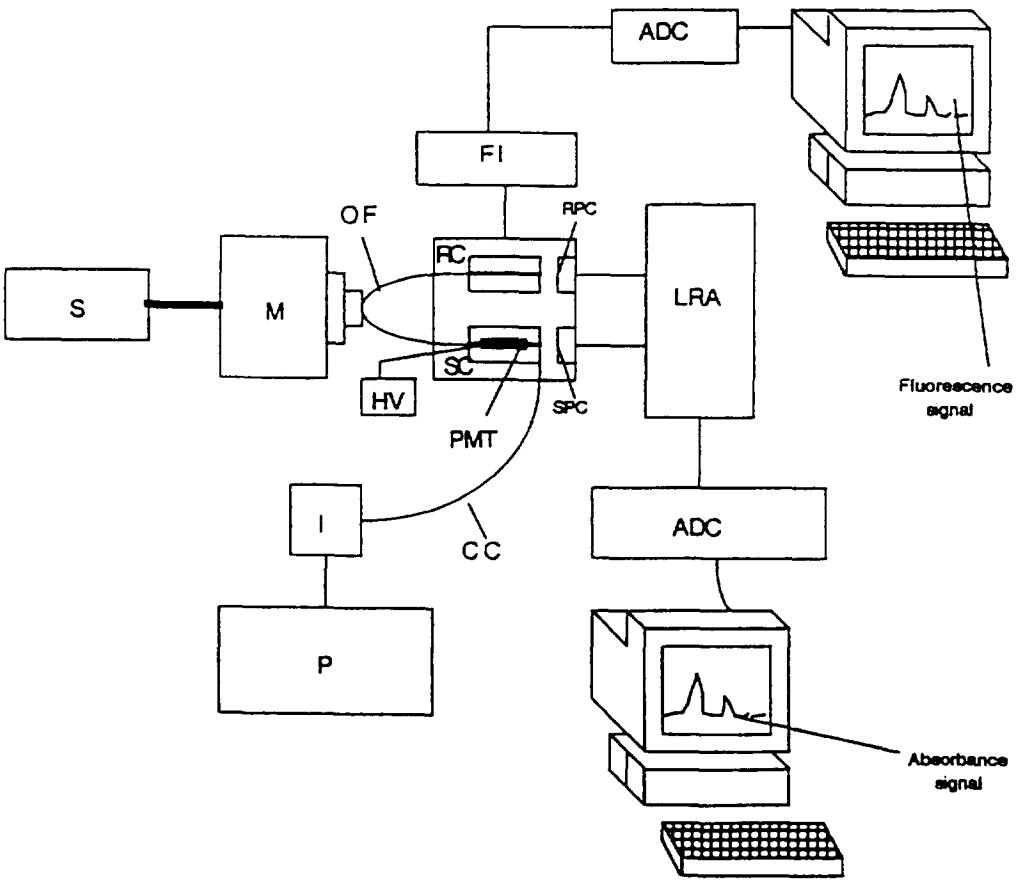

Fig. 5. Experimental setup for simultaneous absorbance and fluorescence measurements. S = Source; M = monochromator; OF = optical fiber; SC and RC = sample and reference cell, respectively; SPC and RPC = sample photocell and reference photocell, respectively; LRA = log ratio amplifier; Fl = fluorometer; PMT = photomultiplier tube; HV = high voltage to the PMT; CC = capillary column; I = injector; P = pump; ADC = analog-to-digital converter.

of noise from a baseline and peak height, were easily performed with this software.

3.5. Chemicals and reagents

Non-chromatographic mobile phases included absolute ethanol (AAPER Alcohol and Chemical Co., Shelbyville, KY, USA), chlorobenzene (MCB Reagents, Cincinnati, OH, USA) and mixtures (with different v/v ratios) of ethanol and chlorobenzene. All mobile phases were reagent grade and were used without further purification. The chromatographic mobile phase consisted of a 92:8 mixture of acetonitrile (Burdick & Jackson Labs., Muskegon, MI, USA) and water (Nanopure, Barnstead, Boston, MA, USA). Perylene and Rhodamine 6G were purchased from Aldrich (Milwauke, WI, USA) and the polynuclear aromatic hydrocarbons were obtained from Chem Services (West Chester, PA, USA).

3.6. Additional instrumentation

All solution refractive indices were measured using a Bausch & Lomb refractometer (Rochester, NY, USA). The absorbance and fluorescence (1 cm pathlength) of Rhodamine 6G solutions were recorded on a Model UV-265 UV–Vis spectrophotometer (Shimadzu Scientific Instru-

ments, Columbia, MD, USA) and a Model 4800C spectrofluorometer (SLM-Aminco), respectively. A Harvard Apparatus (Natick, MA, USA) syringe pump was a substitute for the Varian pump for all of the non-chromatographic flow cell evaluation work.

4. Results and discussion

4.1. Comparison of bend geometries

Three important optical phenomena can be used to characterize the bend geometries. Differences in beam divergence and angular deviation were noted at various mobile phase refractive indices (data not shown). Fig. 3c and d show light decoupling from water-filled lumens in the eccentric and 90° bends, respectively. Note the differences in direction of this decoupled beam for the two bend geometries. Note also differences in beam divergence and light distribution within the beams. While these two phenomena are critical to a complete understanding of flow cell operation, we considered them to be secondary to the ability to efficiently decouple light at the bend. Thus, this third phenomenon (light decoupling) became the most important design consideration for simultaneous absorbance–fluorescence sensing. The eccentric bend capillary flow cell was chosen for all optical and chromatographic evaluations in this work due to its enhanced light decoupling efficiency for a wide range of mobile phase refractive indices. Comparative performance studies of these two flow cell geometries is the subject of a separate publication.

4.2. Detection limits and linearity

The performance of the detector can be judged from its ability to measure small concentrations of analytes and the concentration range over which the detector gives a linear response. We fabricated a variable-pathlength flow cell, whose detection window could be varied by moving the optical fiber (core 116 μm, clad 140 μm, jacket 162 μm) inside the capillary. An eccentric bend capillary with a 250 μm I.D. was used as the flow cell.

Absorbance

Rhodamine 6G solutions ($5 \cdot 10^{-7}$ to $1 \cdot 10^{-4}$ M) were injected into a stream of ethanol through a 60 cm × 250 μm I.D. capillary at a flow-rate of 20.6 μl/min. Visible light at 530 nm and a 5-cm optical pathlength were used for these absorbance measurements. Fig. 6 shows the behavior of absorbance S/N over this range in injected concentration. The injected concentration limit of detection was $1.62 \cdot 10^{-7}$ M ($S/N = 3$) and it was linear over 2.5 orders of magnitude (response index of 0.9716). The sensitivity of the measurement appeared to be shot noise limited. Electronic noise corresponding to ± 0.5 milliabsorbance units (mAU) levels was recorded. These were at least two orders of magnitude higher than those obtainable with commercial detectors. However, the concentration limit of detection is comparable to that reported in the literature for Rhodamine 6G. Planned improvement in this detector design include use of low dark current UV-sensitive photodiodes and a configuration that will allow us to keep the photodetectors as close as possible to the electronics module.

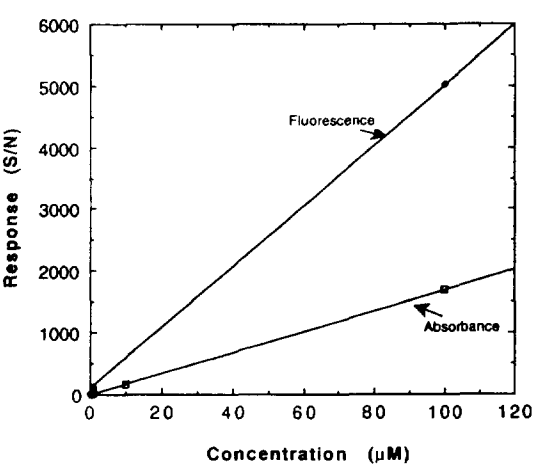

Fig. 6. Variation of absorbance and fluorescence response (S/N) with concentration.

Fluorescence

Perylene solutions from $5 \cdot 10^{-8}$ to $1 \cdot 10^{-4}$ *M* were injected into ethanol at 20.6 μl/min. A cylindrical lens collected fluorescence light from a 2.4-cm region, one edge of which was just outside the fluorescence optical window (see Fig. 4). This placement helped to minimize specular reflections from the optical fiber and scattering effects from the capillary wall. Fluorescence optical window position was optimized for maximum fluorescence signal by making fluorescence measurements at different optical fiber positions inside the capillary flow cell. Fluorescence response for the concentration range studied is also shown in Fig. 6. The concentration limit of detection was $15 \cdot 10^{-9}$ *M* and the response index was 0.8313 for the 3.5 orders of magnitude. Non linear response in fluorescence signal intensity at high fluorophore concentration ($1 \cdot 10^{-4}$ *M*) was observed. We attribute this is to preabsorption filtering along the length of the capillary, i.e. decreasing incident light intensity with increasing distance from the optical fiber. At low analyte concentration this effect is negligible due to very small analyte absorbance. However, as analyte concentration increases propagating incident light decreases exponentially with pathlength as a fundamental consequence of Beer's law.

4.3. Variation of absorbance and fluorescence with flow cell physical pathlength

Absorbance versus pathlength

The pathlength was varied from 1 to 5.8 cm by simply moving the optical fiber relative to the bend. All concentrations of Rhodamine 6G (listed above) were injected for each fixed optical pathlength and the absorbance *S/N* was plotted as a function of analyte concentration. Sensitivity versus pathlength is plotted in Fig. 7a. The slopes of the response curves (sensitivities) increased from $2.9 \cdot 10^{6}$ mAU/*M* for 1 cm pathlength to $19.5 \cdot 10^{6}$ mAU/*M* for 5.8 cm pathlength, an seven-fold increase in sensitivity for a five-fold increase in pathlength. The slope of a log–log plot (not shown) was found to be 1.093. These results clearly indicate that absorbance increases linearly with pathlength, over the range

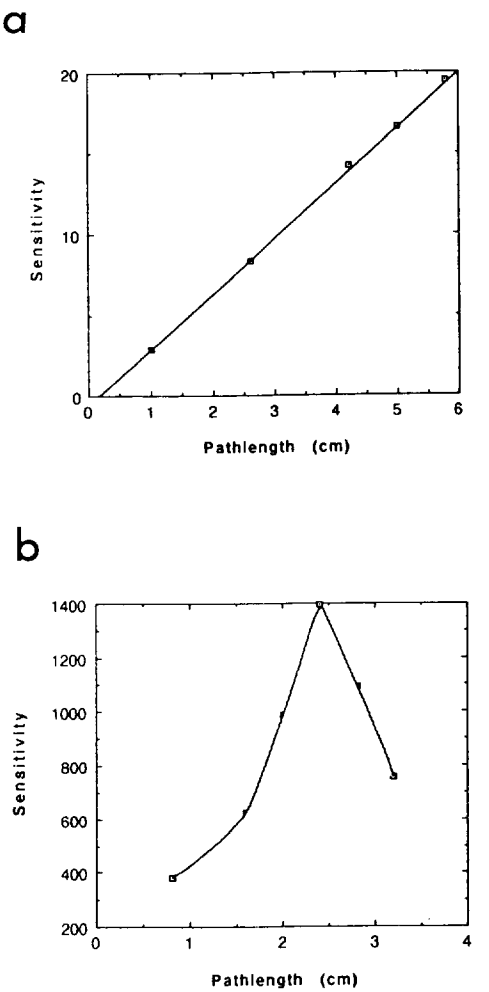

Fig. 7. Variation of detection sensitivity for absorbance (a) and fluorescence (b) with changes in optical pathlength.

of pathlength studied. This experiment indicates Beer's law behavior for small-I.D. axially illuminated capillary flow cells and also verifies that large pathlengths can be used without deviation from linearity neglecting refractive index artifacts. This is not particularly surprising considering that the major light propagation pathway, mode A2, is highly directional (see Theory) and coincident upon the cell's physical pathlength.

Fluorescence versus pathlength

The total fluorescence pathlength that could be obtained was limited to 2.4 cm because of

experimental constraints, i.e. PMT photocathode dimensions and cylindrical lens. Different pathlengths were obtained by moving the optical fiber from 0.8 cm within the fluorescence optical window to 3.2 cm or 0.8 cm beyond that segment of the capillary seen by the PMT. These locations corresponded to distances of 1.8–4.2 cm, relative to the bend. Fluorescence signals for $1 \cdot 10^{-6}$, $1 \cdot 10^{-5}$ and $1 \cdot 10^{-4}$ *M* Rhodamine 6G solutions at each pathlength were obtained. A plot of sensitivity versus pathlength is shown in Fig. 7b. We see that fluorescence sensitivity increases with pathlength from 0.8 to 2.4 cm and then decreases up to 3.2 cm. This decrease in signal is due to the fact that the incident light intensity reaching the fluorophore at the fluorescence optical window is less than the light intensity at the face of the optical fiber. This self absorption phenomenon [32] is more prominent at higher fluorophore concentrations.

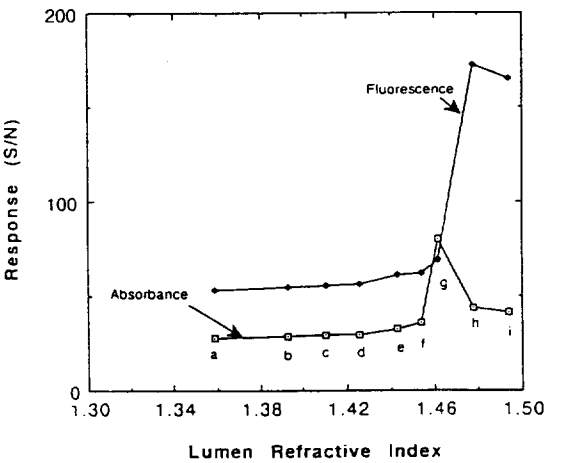

Fig. 8. Variation of absorbance and fluorescence response (*S/N*) with changes in lumen refractive index. Mobile phase refractive indexes: a = 1.3587; b = 1.3930; c = 1.4184; d = 1.4256; e = 1.4340; f = 1.4538; g = 1.4620; h = 1.4774; i = 1.4940.

4.4. Variation of absorbance and fluorescence with lumen refractive index

Ethanol (refractive index 1.3587) and chlorobenzene (refractive index 1.5241) were mixed in various v/v ratios to make nine solutions with refractive indices from 1.3587 to 1.494. A stock solution of $1 \cdot 10^{-3}$ *M* Rhodamine 6G was prepared in ethanol and $1.123 \cdot 10^{-5}$ *M* working solutions were then obtained by diluting the stock solution with the different refractive index diluent solutions (ethanol–chlorobenzene mixtures). Varying concentrations of Rhodamine 6G were injected into each of the nine different refractive index diluent solutions (as mobile phases) in order to study lumen refractive index effects. To isolate these effects on absorbance and fluorescence *S/N*, we divided our capillary flow cell/detector data with normalized optical signals, obtained from standard UV–Vis spectrophotometer and spectrofluorometer measurements, respectively.

Fluorescence

Fig. 8 shows the behavior of absorbance and fluorescence *S/N* over the range of lumen refractive indices studied. The Rhodamine 6G concentration for these measurements was $1.12 \cdot 10^{-5}$ *M*. Notice the gradual increase in *S/N* with refractive index from 1.359 to about 1.462 followed by a rather sharp increase in *S/N* for refractive index 1.4774. Further increases in mobile phase refractive index yielded a small, but significant, decrease in fluorescence *S/N*. The computed value of n_1 (see Theory) for which all light energy would be lumen-confined was found to be 1.4716. For all solutions up to refractive index 1.462 light propagates via mode A where maximum light energy is contained in the capillary wall and lumen. For the 1.4774 and 1.494 refractive index solutions mode B is the primary light propagating mode. The mode transition point, at refractive index 1.4716, is highly correlated with the sharp increase in fluorescence *S/N*. Light-scattering effects in the capillary wall can contribute to the overall *S/N* when mode A predominates over mode B. We have examined the noise data for these measurements and there does appear to be less noise for the two highest refractive index mobile phases. Thus, mode B generates more efficient photonic interactions, since higher signals result from greater incident

light propagation in the lumen and lower noise is present due to less scattering from wall losses associated with mode A. However, less S/N can be seen at mobile phase refractive index significantly greater than 1.4716, as shown in Fig. 8. This is rationally explained as a decrease in the solid angle (see Eq. 10) of light that is emitted from the optical fiber which leads to a decrease in effective pathlength.

Absorbance

A maximum absorbance S/N was recorded for a mobile phase refractive index of 1.4620. Notice the gradual increase in S/N for mobile phases with lower refractive index and the decrease in S/N for mobile phase refractive indexes greater than this value. Compare this decrease in absorbance S/N to the increasing fluorescence S/N in this region of the refractive index scale. Greater fluorescence clearly suggests that the analyte molecules absorbed more light and therefore should have had higher absorbance, as well. We attribute this discrepancy to non-linear photometric phenomena, as follows. If the analyte is a fluorophore and the capillary is a perfect lightguide, deviations from Beer's law can occur [33]. Let

$$A_m = \log (I_r/I_m) \quad (16)$$

and

$$A_s = \log (I_r/I_s) \quad (17)$$

where A_s and A_m are the absorbance readings with and without the sample in the flow cell, respectively. I_r is the light intensity incident on the reference photocell, and I_s and I_m are the light intensities falling on the sample photocell with and without the sample, respectively. The difference, ΔA, or $(A_s - A_m)$ is the absorbance signal due to the sample *only* and is given by

$$\Delta A = \log (I_m/I_s) \quad (18)$$

This equation shows that ΔA will decrease with an increase in I_s. If the flow cell is a perfect lightguide and if the sample is fluorescing and/or scattering, Eq. 18 is written as

$$\Delta A = \log [I_m/(I_s + I_{s'} + I_f)] \quad (19)$$

where $I_{s'}$ and I_f are the light intensities due to scattering and fluorescing, respectively, that strike the sample photocell. In our experiments $I_{s'}$ is considered to be negligible and I_f can be disregarded unless large amounts of fluorescence reach the sample photocell, presumably when the flow cell is a perfect lightguide. Normally, incident light energy that interacts with the fluorophore at the bend is small and the fluorescence signal is negligible. However, when $n_1 >$ 1.4716, the capillary acts as a perfect lightguide and large amounts of fluorophore molecules are excited in the bend region. This results in a non-negligible value of I_f and a concomitant *decrease* in absorbance.

Fig. 9 is a plot of the baseline absorbance signal as a function of n_1. Notice the negative values on the ordinate. The absolute absorbance values are not nearly as important as the overall trend. More negative baseline absorbances indicate greater amounts of light exiting at the bend. Since incident light intensity is fixed, a higher light intensity at the sample photocell is possible

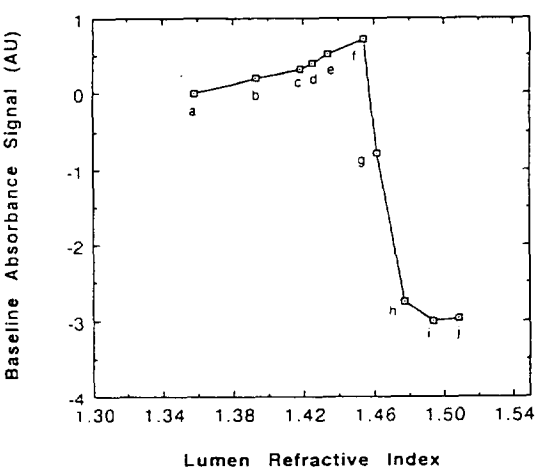

Fig. 9. Baseline absorbance signal (AU) as a function of lumen refractive index. Mobile phase refractive indexes as in Fig. 8 plus j = 1.5087.

only if more light actually propagates from the optical fiber to the bend and completely decouples at the bend. In the region from lumen refractive indexes of 1.359 to 1.454 a gradual increase in baseline absorbance is seen. This corresponds to *less* light arriving at the sample photocell which we correlate with the fact that the capillary actually becomes a less-efficient lightguide as n_1 approaches n_w (1.458) due to more light escaping into the wall. Recall that $R = 0$ when $n_1 = n_w$. At $n_1 = 1.462$, n_w is exceeded and significantly negative baseline absorbance readings are observed. Here, there is an improvement in lightguiding capability of the capillary flow cell. This trend continues, dramatically up to $n_1 = 1.4774$ and much less dramatically up to 1.494. Better flow cell performance is indicated within the 1.49 to 1.50 refractive index range since the combined effects of more efficient lightguiding within the capillary and significant light decoupling at the bend can explain the features in this region of the plot. A slight increase in baseline absorbance is observed at $n_1 = 1.509$. This is likely due to the fact that some light rays are now able to travel across the bend, therefore less light strikes the sample photocell and the absorbance is higher.

The results shown in Fig. 9 present important implications regarding absorbance detection for gradient micro-LC. If the mobile phase refractive index varies from 1.359 to 1.4538 there will be a baseline shift in the absorbance signal that follows two trends, points a to c and points c to f. In the first region the slope is 5.4 mAU/mRIU (millirefractive index units) and the slope is 11.3 mAU/mRIU in the second region. These features probably represent a single exponential curve, within the precision of the experiment. For a typical 0 to 100% acetonitrile/water gradient, the refractive index change is approximately 10 mRIU (data not shown.) Therefore, such a gradient would produce a baseline change of about 54 mAU, a significant amount indeed compared to amplitudes of typical analyte peaks at low concentration. The specific optical effects responsible for this artifact have been identified and discussed above. Logically, then, there are optical techniques which might be employed to minimize their impact. This is the subject of our current research in this area.

4.5. Influence of capillary wall thickness on absorbance and fluorescence signals

Two capillary flow cells, with similar inner diameter (approximately 100 μm) but different wall thicknesses (67 and 261 μm), were evaluated. Solutions of Rhodamine 6G ($1.12 \cdot 10^{-4}$, $1.12 \cdot 10^{-5}$ and $1.12 \cdot 10^{-6}$ M) were used for absorbance and solutions of perylene ($1 \cdot 10^{-4}$, $1 \cdot 10^{-5}$ and $1 \cdot 10^{-6}$ M) were used for fluorescence measurements. An ethanol mobile phase was pumped at 20 μl/min in all cases. Absorbance measurements were performed at 530 nm and 434 nm excitation light was used for fluorescence measurements. For both wavelengths, light was launched into the flow cell capillaries with a 50-μm core diameter optical fiber. Fig. 10 shows plots of detector response versus analyte concentration for both types of measurements and detector flow cells. Compare the slopes of the response plots for each of the measurement types and wall thicknesses. Absorbance sensitivity increased by a factor of 1.16 as the wall thickness decreased from 261 to 67 μm. Similarly, fluorescence sensitivity increased by a factor of 1.21 for the same wall thickness

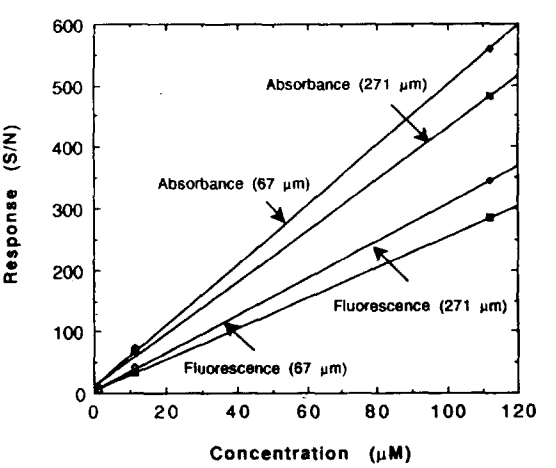

Fig. 10. Absorbance and fluorescence response (S/N) for 100 μm I.D. capillaries with two different wall thickness, 76 and 271 μm.

values. Even though this is not a significant sensitivity enhancement with decreasing wall thickness, a higher S/N is achieved for *both* absorbance and fluorescence. A smaller wall thickness results in less wall propagation, reducing the contributions of losses in the wall (such as scattering and absorption).

4.6. Polynuclear aromatic hydrocarbon micro-LC

A reversed-phase micro-LC separation of a seven-component polynuclear aromatic hydrocarbon mixture was used to further illustrate utility of the flow cell. The mobile phase, acetonitrile–water (92:8), was pumped at a flow-rate of 5 μl/min. A 2.2-cm optical pathlength was used to generate the fluorescence chromatogram shown in Fig. 11. Only fluorescence measurements were made since the silicon photocells had very poor UV response. The inset of Fig. 11 shows a chromatogram close to the detection limit. The analytical figures of merit for these polynuclear aromatic hydrocarbons are listed in Table 1. These concentrations (at $S/N = 3$) are two orders of magnitude better than what we have achieved in the past [34], using cross-beam illumination, photon-counting electronics and higher laser power at the flow cell (1 mW). The peak labelled c in Fig. 11 is due to two coeluting analytes (chrysene and 1,2-benzanthracene). Peak identifications were confirmed by spiking a low concentration (10^{-8} M) mixture with individual analytes of higher concentration (10^{-5} M). We also studied the effect of optical detector window length on overall detectability in polynuclear aromatic hydrocarbon separation. The optical window length was varied from 0.09 to 2.2 cm. The resulting chromatograms are shown in Fig. 12. With increasing length of the fluorescence window, the detectability for pyrene and

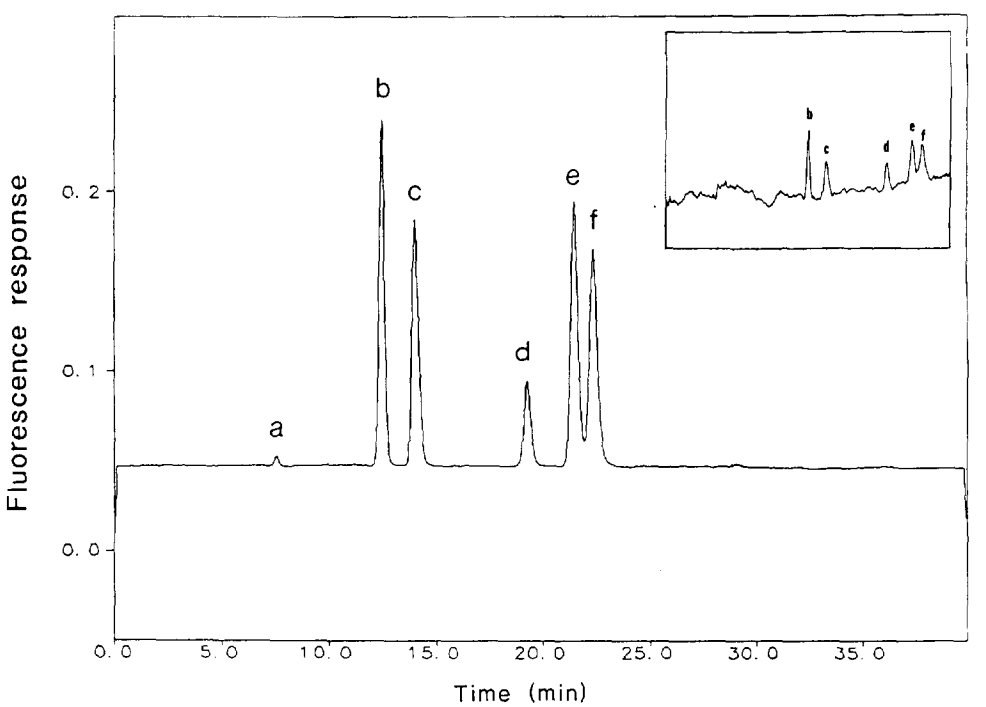

Fig. 11. Laser-induced fluorescence micro-LC chromatograms of a seven-component mixture of polynuclear aromatic hydrocarbons. Peaks: a = 1,2-benzofluorene; b = pyrene; c = chrysene and 1,2-benzanthracene; d = perylene; e = 1,2-benzopyrene; f = 1,2,5,6-dibenzanthracene. Inset shows chromatogram close to the detection limit.

Table 1
Analytical figures of merit for polynuclear aromatic hydrocarbons

Polynuclear aromatic hydrocarbons	MIC (M)	MIQ (g)
1,2-Benzofluorene	$4.8 \cdot 10^{-7}$	$10.4 \cdot 10^{-12}$
Pyrene	$2.1 \cdot 10^{-8}$	$433 \cdot 10^{-15}$
Perylene	$1.4 \cdot 10^{-8}$	$343 \cdot 10^{-15}$
1,2-Benzopyrene	$1.6 \cdot 10^{-8}$	$406 \cdot 10^{-15}$
1,2,5,6-Dibenzanthracene	$1.6 \cdot 10^{-8}$	$456 \cdot 10^{-15}$

MIC and MIQ are the minimum injected concentration and minimum injected quantity, respectively, at $S/N = 3$.

perylene increased by a factor of 4 while their separation efficiencies decreased by factors of only 1.2 and 1.1 for pyrene and perylene, respectively. Obviously the chromatographic peak width is greater than the largest detector volume represented. This flow cell design allows such changes (optical window length) to be easily made, enabling optimum performance to be achieved for a given capillary volume and analytical separation.

5. Conclusions

We have shown some of the optical sensing capabilities of a unique eccentric bend axial-illumination capillary flow cell. The light-propagation pathways in such a device have been evaluated as a function of lumen refractive index and capillary wall thickness. At low mobile phase refractive index, typical of reversed-phase LC, light propagation in the flow cell is highly

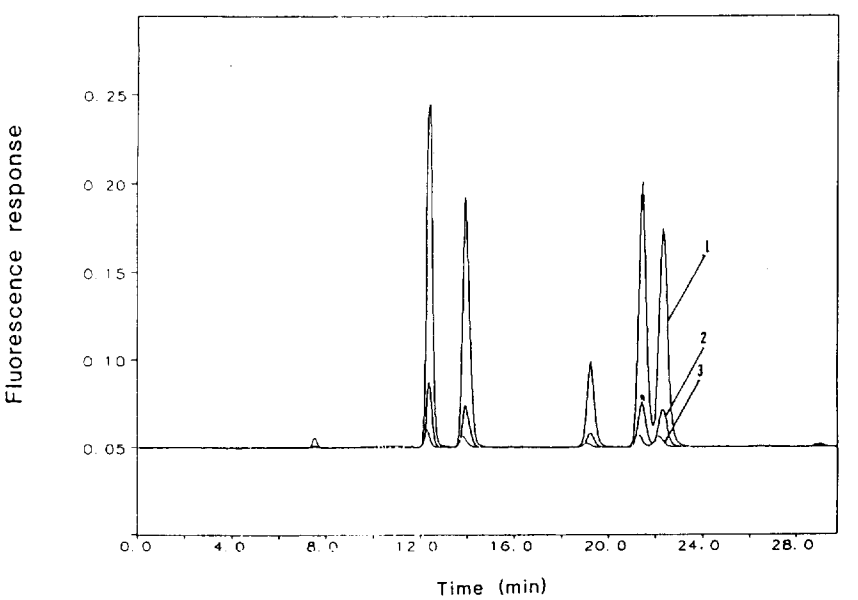

Fig. 12. Laser-induced fluorescence micro-LC chromatograms with three different optical window lengths. Window lengths: 1 = 2.2 cm; 2 = 0.27 cm; 3 = 0.09 cm.

directional and light can be very efficiently decoupled at the bend. Both absorbance and fluorescence sensing, with extended pathlengths, are possible with this design. Pathlengths up to 5 cm and enhanced detection sensitivities have been demonstrated. The flow cell is compatible with micro-LC and analytical performance is two orders of magnitude better than our previous results [34]. With a volume of 173 nl, the 2.2 cm long $\times$ 100 μm I.D. cell is far too large for capillary electrophoresis. Smaller versions are possible, however, using smaller optical fiber–capillary combinations as well as shorter pathlengths. Perhaps this design will also enable refractive index sensing. Work is underway to verify this. The potential for simultaneous absorbance, fluorescence and refractive index detection for micro-LC is alluring.

Acknowledgements

We gratefully acknowledge the assistance of Harvey Bellamy in obtaining the flow cell photographs in Fig. 3. We also thank Professor Dominick Casadonte for use of the plastic sheet cut-off filters. Travel support for A.A. Abbas was provided by the Embassy of the United Arab Emirates. Support for poster preparation was partially provided by a grant from Westinghouse-Hanford Co., Richland, WA, USA.

References

[1] M.V. Novotny and D. Ishii (Editors), *Microcolumn Separations —Columns, Instrumentation and Ancillary Techniques*, Elsevier, Amsterdam, New York, 1985.
[2] D. Ishii, *Introduction to Microscale High-Performance Liquid Chromatography*, VCH, New York, 1988.
[3] K. Jinno and C. Fujimoto, *LC·GC*, 7 (1989) 328.
[4] F. Yang, *J. High Resolut. Chromatogr. Chromatogr. Commun.*, 4 (1981) 83.
[5] E.J. Guthrie and J.W. Jorgensen, *Anal. Chem.*, 56 (1984) 483.
[6] S. Einarsson, S. Folestad, B. Josefsson and S. Lagerkvist, *Anal. Chem.*, 58 (1986) 1638.
[7] F. Yang, *J. Chromatogr.*, 236 (1982) 265.
[8] M. Janecek, F. Foret, K. Šlais and P. Boček, *Chromatographia*, 25 (1988) 815.
[9] Y. Hirata and M. Novotny, *J. Chromatogr.*, 186 (1979) 521.
[10] C. Borra, D. Wiesler and M. Novotny, *Anal. Chem.*, 59 (1987) 339.
[11] V.L. McGuffin, in P. Sandra and W. Bertsch (Editors), *Proceedings of the 6th International Symposium on Capillary Chromatography*, Hüthig, Heielberg, 1985, p. 800.
[12] T.J. Edkins and D.C. Shelly, in G. Patonay (Editor), *HPLC Detection: Newer Methods*, VCH, New York, 1992, p. 13.
[13] K. Fujiwara, J.B. Simeonsson, B.W. Smith and J.D. Winefordner, *Anal. Chem.*, 60 (1988) 1065.
[14] K. Tsunoda, A. Nomura, J. Yamada and S. Nishi, *Appl. Spectrosc.*, 43 (1989) 49.
[15] K. Tsunoda, A. Nomura, J. Yamada, S. Nishi and I. Kojima, *Nippon Kaguka Kaishi*, 1989 (1989) 233.
[16] J.P. Chervet, M. Ursem, J.P. Salzmann and R.W. Vannoort, *J. High Resolut. Chromatogr., Chromatogr. Commun.*, 12 (1989) 278.
[17] I.H. Grant and W. Steuer, *J. Microcol. Sep.*, 2 (1990) 74.
[18] X. Xi and E.S. Yeung, *Anal. Chem.*, 62 (1990) 1580.
[19] X. Xi and E.S. Yeung, *Appl. Spectrosc.*, 45 (1991) 1199.
[20] J. Taylor and E.S. Yeung, *J. Chromatogr.*, 550 (1991) 831.
[21] J.V. Sweedler, J.B. Shear, H.A. Fishman and R.N. Zare, *Anal. Chem.*, 63 (1991) 496.
[22] J.P. Chervet, R.E.J. van Soest and M. Ursem, *J. Chromatogr.*, 543 (1991) 439.
[23] K. Fujiwara, S. Riekojyo, H. Tsubota and R.L. Carter, *Appl. Spectrosc.*, 46 (1992) 1032.
[24] J.A. Taylor and E.S. Yeung, *Anal. Chem.*, 64 (1992) 1741.
[25] A.A. Abbas and D.C. Shelly, *J. Chromatogr.*, 631 (1993) 133.
[26] S.E. Moring and R.T. Reel, *Anal. Chem.*, 65 (1993) 3454.
[27] T. Wang, J.H. Aiken, C.W. Huie and R.A. Hartwick, *Anal. Chem.*, 63 (1991) 1373.
[28] E. Hecht, *Optics*, Wesley, Reading, MA, 1987, Ch. 4, p. 79.
[29] J.R. Gant and P.A. Perrone, *Am. Lab.*, 17 (1985) 104.
[30] S.A. Wilson and E.S. Yeung, *Anal. Chem.*, 57 (1985) 2611.
[31] T.J. Edkins and D.C. Shelly, *J. Chromatogr.*, 411 (1987) 185.
[32] D.C. Harris, *Quantitative Chemical Analysis*, Freeman, New York, 1987, Ch. 20, p 524.
[33] J.R. Lackowicz, *Principles of Fluorescence Spectroscopy*, Plenum, New York, 1983, Ch. 2, p. 48.
[34] T.J. Edkins and D.C. Shelly, *J. Chromatogr.*, 459 (1988) 109.